Jurnal Teknologi

Full Paper

NUMERICAL SIMULATION ON THE TENSILE STRAIN HARDENING BEHAVIOUR OF ENGINEERED CEMENTITIOUS COMPOSITES (ECC)

Chee Zheng Woo[a], Wee Teo[a], Kazutaka Shirai[b]

[a]School of Energy, Geoscience, Infrastructure and Society (EGIS), Heriot-Watt University Malaysia, 62200 Putrajaya, Malaysia
[b]Faculty of Engineering, Hokkaido University, Sapporo 060-8628, Japan

Article history
Received
21 March 2022
Received in revised form
7 July 2022
Accepted
18 July 2022
Published Online
23 October 2022

*Corresponding author
t.wee@hw.ac.uk

Graphical abstract

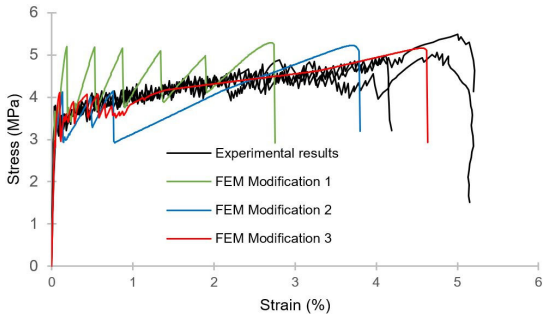

Abstract

Numerical simulation for evaluating tensile strain hardening behaviour of engineered cementitious composites (ECC) materials are extremely limited. This paper presents a finite element (FE) model developed to determine the multiple-cracking and strain hardening behaviour of ECC under uniaxial tension. A nonlinear FE program, ATENA was used in this study. A constitutive law based on individual crack-based model derived by the traction-separation relationship, or also known as tensile function was implemented in the model. Model calibration with parameter modifications were illustrated. The final simulation result predicts accurately the experiment tensile stress strain curves, including the tensile strain hardening response, ultimate tensile strength and tensile strain capacity. This includes validation from ECC specimens tested by various researchers. It has found that accuracy of the model is improved by lowering the crack opening displacement corresponds to the first cracking. The finding from this study would be useful in the future for further parametric analyses and structural optimization design of ECC members.

Keywords: Engineered cementitious composites (ECC), strain hardening behaviour, finite element modelling

1.0 INTRODUCTION

Concrete is made up of cement, aggregates (coarse and fine) and water. It is one of the most commonly used construction materials worldwide. However, major mode of weaknesses associated to concrete are their quasi-brittle behaviour, low tensile strength, ductility and toughness. All these characteristics could lead to deterioration issues and failures of the concrete structures. Over the years, several efforts and interests have been significantly researched to improve the ductility, tensile performance and toughness of the concrete materials.

Engineered cementitious composites (ECC), also referred to as Strain Hardening Cementitious Composites (SHCC) is one of the promising materials for enhancing the concrete behaviour in terms of durability and ductility. ECC was originally developed by Li *et al*. (1992, 1993, 1998) [1-3], to overcome the brittleness of conventional concrete matrix. It possesses superior tensile strain capacity of more than 3%, which is more than 500 times greater than

normal concrete by adding fibres with volume fraction of 2% (or less) to the matrix [4-5]. ECC exhibits high energy absorption and excellent strain hardening with multiple fine cracking, which make it highly suitable for structures design against severe loading, such as seismic, impact and blast. The enhanced mechanical properties are greatly attributed to the systematic micromechanics-based design approach on the fibre matrix interface properties.

To date, most of the research on ECC have been primarily experimental studies in material development and characterization [6-10]. For that reason, uniaxial tensile tests are the common test setup widely used to evaluate the tensile performance of the specimens. There are many different types of test specimen shapes adopted, but the most popular is the dogbone-shaped size and geometry according to JSCE recommendations [24], as later shown in Figure 4. It is well recognised that uniaxial tensile tests are rather challenging to be maintained in consistent quality control, and interpreted consistency in results [11].

Numerical analyses such as finite element method (FEM) offers an attractive approach to complement experimental works. It could help to overcome difficulties on production time, cost, handling and testing. Also, it could address specific details that are hard to capture experimentally, such as fibre-matrix interface properties and behaviour. Studies of numerical simulation for evaluating tensile strain hardening characteristics of ECC materials are extremely limited in comparison with experimental investigation.

Huang *et al*. (2016) [12] conducted an extended finite element method (XFEM) to stimulate the tensile strain hardening and multiple cracking behaviour of ECC using ABAQUS [13] under uniaxial tension. The material randomness of matrix flaw and fibre distribution were both considered in the model. The crack is modelled using the cohesive zone model with a simplified cohesive constitutive model accounting for the matrix and fibre bridging effect. The computed tensile strength and tensile strain capacity shown good agreement with the test results, especially when material randomness is taken into account.

Kabele (2002) [14] proposed a homogenization-based constitutive model for ECC material that exhibits multiple cracking. The constitutive law is obtained as the relationship between overall stress and overall strain of a representative volume element (RVE). Although this approach has proven to be accurate and capable of predicting well the global load-displacement response and load carrying capacity of ECC members. But it could lead to unrealistic high stiffness before the peak load especially in members failing in shear-tension mode [15]. Realizing the inaccuracy, Kabele [16] extended his work by considering the behaviour of individual crack in the model. This approach shown to provide more accurate representative to the experimental results.

In this paper, a nonlinear finite element program ATENA was used to evaluate the tensile strain hardening and multiple cracking behaviour of ECC under uniaxial tension. The crack is modelled based on the individual crack-based model proposed by Kabele [16] using the traction separation law defined by relationship between the bridging traction and relative crack opening displacement, which represents the cohesive effect of cracks of matrix and fibre bridging response. Parametric analyses including tensile function was carried out under uniaxial tensile loading condition. A model calibration technique was used to define the tensile function. The proposed calibration technique was validated using the experimental results obtained from various researchers to evaluate the effectiveness of the numerical simulation approach.

2.0 METHODOLOGY

2.1 Tensile Strain Hardening Behaviour

The strain hardening behaviour of a cementitious composites is a phenomenon characterised by the interaction between the matrix, fibre and its interface. Figure 1 shows the tensile stress strain curve of ultra-high performance fibre reinforced concrete (UHPFRC), which also has similar tensile characteristic to ECC under uniaxial tension.

According to Naaman and Reinhardt [18], the strain hardening composites is a material where the tensile strength σ_{pc} exceed the matrix cracking strength σ_{cc}, which satisfies the micromechanics strength criterion developed by Li [19]. The matrix cracking strength is influenced by the matrix fracture toughness and initial flaw size to initiate a crack, where the matrix fracture toughness is assumed to be uniform throughout the specimen and flaw size varies from one space to another. As the tensile load applied to the specimen, the area which has the most favourable oriented flaw causes the crack initiation to be started and continuously works towards small flaws.

On each of the microcracks formed, the load after cracking is carried by the fibre bridging capacity in the matrix-fibre interface, where fibre bridging capacity varies from one microcracks to another due to its non-uniformly dispersion of fibre throughout the specimen. In the other word, the load carried by the fibre bridging is a function of the crack opening governed by tensile stress strain relationship that increases to a peak as shown in Figure 1. As a result, multiple cracking is formed when the process of fibre bridging progressively works as the tensile load increases until a peak value of tensile strength is reached, termed as the strain hardening capacity.

The pseudo strain hardening (PSH) strength index which determines the margin difference between

the ultimate tensile strength σ_{pc} and the matrix cracking strength σ_{cc} define the performance and result of multiple cracking and tensile strain hardening behaviour of the material [20]. A higher PSH index indicates a greater performance in tensile strain hardening behaviour and a higher possibility of saturated multiple cracking, thus results in a greater tensile ductility of the material.

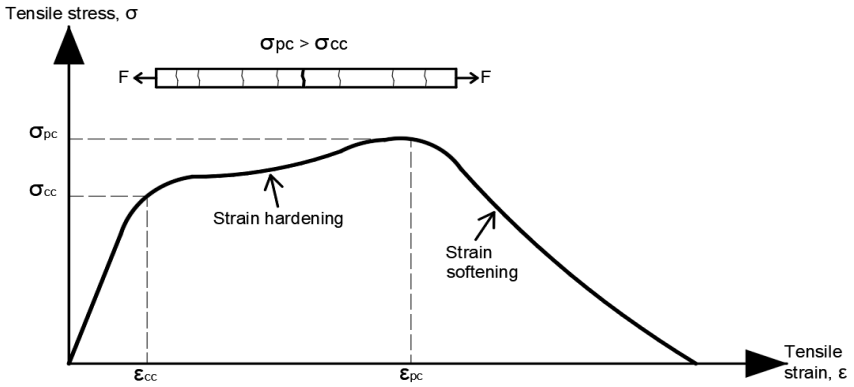

Figure 1 Typical tensile stress strain hardening behaviour of UHPFRC materials. [18]

2.2 Individual Crack-Based Model

Figure 2 shows the traction separation law defining the relationship between the bridging traction and relative cracking opening displacement proposed by Kabele [16], which is implemented in this study. It represents the cohesive effect on cracks of matrix and fibre bridging response. The brittleness behaviour of matrix itself is determined by linear tension-softening relationship governed by two parameters: matrix cracking strength σ_{cc} and crack opening displacement which the matrix cohesive stress is completely released δ_{co}. The function of this matrix traction separation can be expressed as [16]:

$$\sigma_{ts,M}(\delta_n) = \sigma_{cc}\left[1 - \left(\frac{\delta_n}{\delta_{co}}\right)\right] \quad (1)$$

where $\delta_n \leq \delta_{co}$; σ_{cc} is the stresses corresponding to crack opening displacement δ_n. For the hardening part of traction separation law of fibre bridging after the matrix traction separation, the function can be defined as:

$$\sigma_{ts,F}(\delta_n) = \sigma_{pc}\left(\frac{\delta_n}{\delta_{pc}}\right)^{\frac{1}{2}} \quad (2)$$

where $\delta_n \leq \delta_{pc}$; σ_{pc} is the ultimate tensile stress carried by the fibre bridging capacity corresponding to crack opening displacement δ_{pc}. The traction separation law at which the post peak of σ_{pc} represents the gradual loss of fibre bridging capability due to fibre pullout. This traction separation law is defined by assuming linear softening expressed as:

$$\sigma_{ts,F}(\delta_n) = \sigma_{pc}\left[1 - \left(\frac{\delta_n - \delta_{pc}}{\delta_u - \delta_{pc}}\right)\right] \quad (3)$$

where $\delta_{pc} \leq \delta_n \leq \delta_u$; δ_u is the crack opening displacement at which the fibre bridging is completely debonded. The total traction separation law for the crack opening can be simplified by summing up Eqs. (1) and (2) or (3):

$$\sigma_{ts}(\delta_n) = \sigma_{ts,M}(\delta_n) + \sigma_{ts,F}(\delta_n) \quad (4)$$

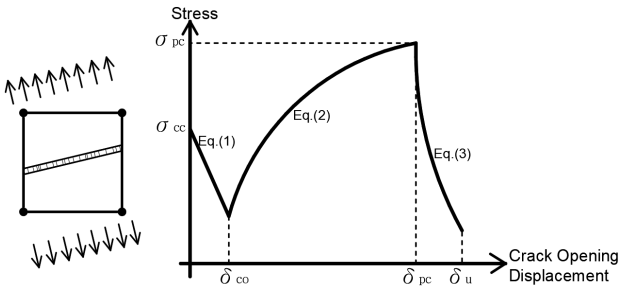

Figure 2 Typical individual crack-based concept

2.3 Numerical Simulation

2.3.1 *Finite Element Implementation*

ATENA (v 5.7) [21] was used along with GiD (v 14.0.5) to stimulate the tensile strain hardening behaviour of dogbone-shape specimen in the present study. ATENA uses fracture-plastic law for both tensile and compression response. The approach of the tensile or the fracture modelling was based on smeared crack concept and Rankine failure criterion with the fixed crack model implemented following the principal stress directions at onset of cracking. The material response, damage and failure stimulated by computational model were highly depended on the quality of material model which defined the quality and accuracy of stimulated results.

In this study, "*Cementitious2SHCC*" material model was used, which is suitable for determining the tensile strain hardening response. The theory behind this material model is identical to stress strain

relationship in uniaxial tension described in fib Model Code 2010 [11]. The stress strain constitutive law in uniaxial tension defined such that introduction of characteristic length is required for a structural element, where the continuous mechanics is governed by stress strain law and fracture mechanics is governed by crack opening relationship.

2.3.2 Tensile Function

In the fracture model, each crack is represented on the finite element level and its response is characterized by the traction-separation relationship, or also known as tensile function. It is based on the individual crack-based approach where it describes the evolution of tensile stresses in one finite element after crack formation, even in multiple cracking condition. A crack is perceived as a displacement discontinuity, which is capable of transferring stress between its faces. This cohesive stress is related to the crack opening displacement through a traction-separation relationship. Traction force transmitted across the cracks are usually characterised by bridging effect of matrix-fibre for the model.

Tensile function is expressed in the model as relationship between tensile stresses versus fracture strains, as illustrated in Figure 3. The fracture strain ε_f can be calculated by the following equation [17].

$$\varepsilon_f = \frac{\delta_n}{L_t} \quad (5)$$

where δ_n is the crack opening width and L_t is the characteristic length. It is noteworthy that characteristic length L_t is a material parameter and can be taken as equal to the size of the element.

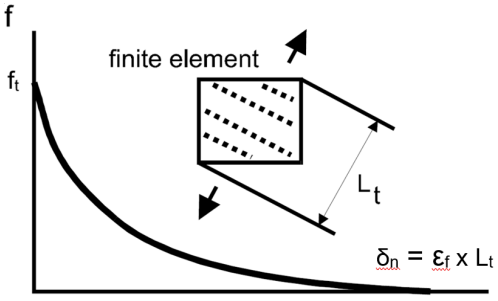

Figure 3 Tensile stress-crack opening and characteristic length

Equation (4) is implemented in the crack response of the fracture model with each finite element associated with a single crack. The formation for this crack will undergo a sudden stress drop before it captures the hardening effect as shown in Figure 2, reflecting the response of a single crack in ECC. When this approach is used for simulating the strain hardening behaviour of ECC with multiple cracks, the FE size in the domain where multiple cracking is achieved is taken as the minimum spacing between cracks. When carrying out the simulation on uniaxial tensile test, the model will uniformly capture all the stress field such as the cracking stress. It may not uniformly apply to all elements, but it would cause cracking to all element simultaneously [22].

2.3.3 Experimental Tests and Results

The FE model is calibrated using uniaxial tensile test results from specimen P20 described in the earlier work by Yu *et al*. [23]. This specimen was produced using ECC with 2% volume fraction of PVA fibres. The matrix parameters such as the elastic modulus, compressive strength and fibre properties used in the model were taken directly from the test results [23].

Table 1 summarise the mix proportions utilised in the study. Polyvinyl alcohol (PVA) fibre (REC15, Japan) was used as a reinforcing fibre to enhance the ductility of the specimen. The mechanical properties of the PVA fibre are shown in Table 2. For more details on the chemical composition and physical properties of the mixture are advised to refer to Yu *et al*. [23] paper.

The test specimen has a dogbone-shaped, as shown in Figure 4, according to JSCE recommendations [24]. Uniaxial tensile tests were carried out by placing the specimen with a chuck at its end, a fixed support at one end and a hinge support at the other end. Two linear displacement transducer (LVDT) were attached to the specimen along the gauge length of 80mm to determine the deformation after the load is applied.

Table 1 Composition and mix proportion of ECC specimen [23]

Specimen	Binder (B)				W/B	S/B	SP/B	PVA
	OPC	FA	LSP	SAC				
P20	0.196	0.72	0.08	0.004	0.3	0.2	0.0037	0.02

Note: OPC: Ordinary Portland Cement; FA Fly ash (ASTM C168 Class F); LSP: Limestone powder; SAC: Calcium sulfoaluminate cement; W; Water; S: Silica sand; PVA; Kuraray K-II REC 15 polyvinyl alcohol fibres.

Table 2 Mechanical properties of PVA fibre

Diameter (μm)	Length (mm)	Density (g/cm3)	Tensile Strength (MPa)	Elastic Modulus (GPa)
39	12	1.3	1275 - 1620	16.9

Table 3 Summary of mechanical properties of P20 specimen [23]

Specimen	Mechanical Properties				
	Elastic Modulus, E_m (GPa)	Compressive Strength, f_c (MPa)	Tensile Strength, σ_{pc} (MPa)	Tensile Strain, ε_{pc} (%)	Average Crack Width (μm)
P20	14	36	5.17	4.63	< 60

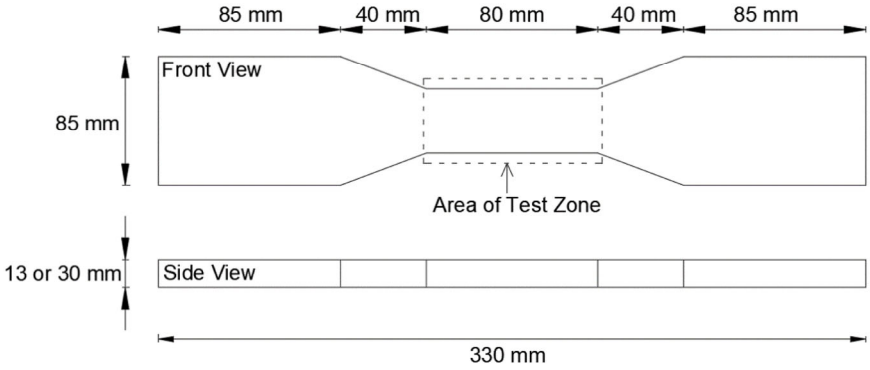

Figure 4 Specimen geometry for uniaxial tensile test

The mechanical properties test results are summarised in Table 3. The obtained tensile stress strain curves under uniaxial tensile are presented in Figure 5. It is observed that the specimen shows an excellent performance in term of tensile strain capacity which is more than 4% with an average crack width of less than 60 μm.

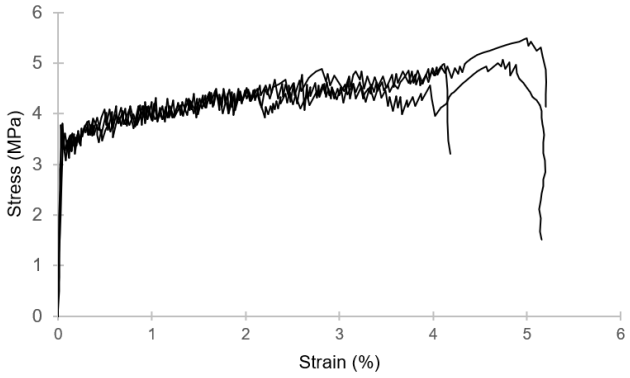

Figure 5 Experimental stress strain curves. [23]

2.3.4 Analysis Procedures

FE modelling on the P20 specimen under uniaxial tensile test was carried out using hexahedral mesh with 32 elements over the 80 mm length of tested region, which mesh size equal to 2.5 mm. A further mesh refinement study was carried out to understand the overall response between models with different mesh sizes in later section. A 20 mm thick with elastic properties material was used on the loading and supporting plate. A static loading rate of 3.3 x 10^{-6} mm/s was used to carry out FE analysis which the loading rate is similar to the experiment. The input parameters such as elastic modulus, compressive strength and tensile strength are depicted in Table 3. The FE model and setup condition are shown in Figure 6.

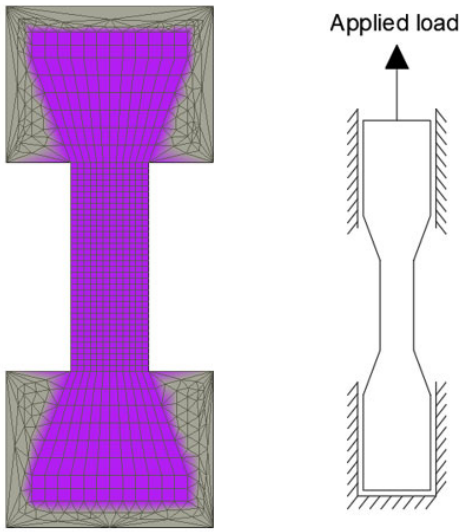

Figure 6 FE model and setup condition for the simulation

The modelling procedure on the tensile strain hardening behaviour are described as follow based on ATENA handbook [17]:

1. Two model parameters are crucial in the modelling, a) ultimate tensile strength, and b) tensile function. Initial setup tensile strength value, which describe the ultimate tensile strength of the model are obtained directly from experimental results (Table 3). Tensile function is the traction-separation relationship. It is represented by σ_f/σ_{pc} parameter on the vertical axis and ε_f parameter on the horizontal axis.
2. Carry out the analysis, export and compare the simulated data with the experimental results in term of stress strain diagram.
3. If the difference between both simulated and experimental results is in good agreement, the determination of model parameters is acceptable. Otherwise, the tensile function parameters should be modified to obtain better results. These steps are repeated until the results satisfactory as compared with experimental results.

2.3.5 *Parameter Modification*

Parameter ε_f and σ_f/σ_{pc} in tensile function are adjusted accordingly to closely represent to the actual tensile hardening and softening behaviour. In the following sections, three stages of modification on the tensile function parameters are illustrated.

a) Modification 1

Table 4 shows the proposed values for the initial parameter ε_f and σ_f/σ_{pc} used in the first stage of the analysis. Also included in the table is the graphical plot of those values.

Point 1 [0.0, 1.0] represent the matrix cracking strength, σ_{cc} as show in Figure 2. As starting, the initial value is assumed equal to ultimate tensile strength σ_{pc}, thus parameter σ_f/σ_{pc} = 1.0.
Point 3 [0.024, 1.05] represent the ultimate strain hardening stage. The fracture strain parameter ε_f is 0.024, calculated from experimental average crack width of 60 µm (see Table 3) based on Equation (5). Parameter σ_f/σ_{pc} is taken as 1.05, assuming 5% strain hardening increment.
Point 2 represent the condition when matrix cohesive stress achieved crack opening displacement δ_{co}, see Figure 2. At initial analysis, it is unknown thus values are assumed at 50% matrix cracking strength and fracture strain of 0.0015.

Figure 7 shows the simulated tensile stress strain curve using the proposed parameters from Table 4. The corresponding experimental curves are also plotted for comparison. It is observed that the simulated curve did not perform well in term of the first cracking strength, strain hardening part and the strain capacity. This mean further modifications are required to improve the accuracy of the calibration.

Table 4 Parameter ε_f and σ_f/σ_{pc} for modification 1

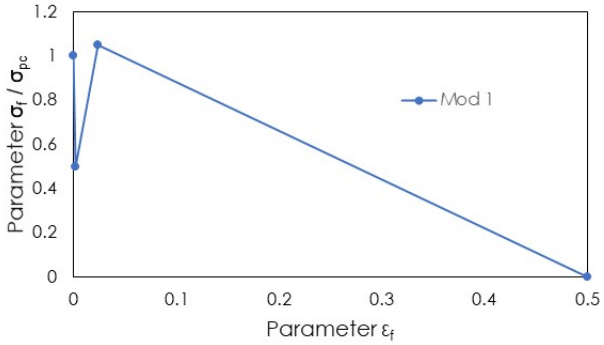

Point	Parameter ε_f	Parameter σ_f/σ_{pc}
1	0.0	1.0
2	0.0015	0.5
3	0.024	1.05
4	0.5	0

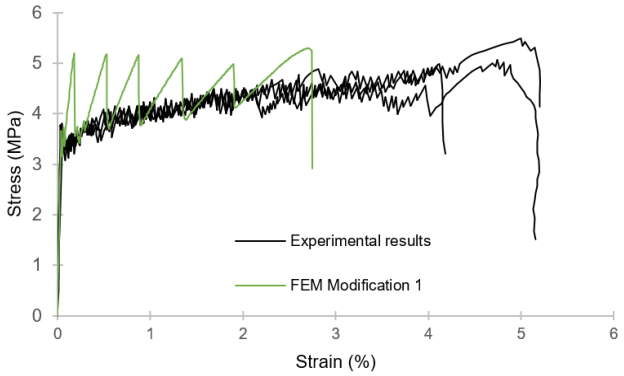

Figure 7 Comparison of tensile stress strain curves with parameter modification 1

b) Modification 2

As shown in Figure 7, the first cracking strength for simulated curve from parameter modification 1 is approximately 5.1 MPa, which is about 20% higher than the experimental curve. Modification on the matrix cracking strength need to be done on point 1 of the tensile function. Thus, it is proposed *Point 1* is lower to [0.0, 0.8].

The simulated model (based on modification 1) obtained an average crack width of 6.2 µm after first cracking strength attained. Thus, the fracture strain parameter ε_f at point 2 would be revised to 0.0025 calculated from Equation (5). On the other hand, the parameter σ_f/σ_{pc} would be increased approximately 10% to account for lower simulated stresses than in experiment at each subsequent stress drops due to cracking. The revised *Point 2* is therefore becoming [0.0025, 0.55].

The parameter ε_f at point 3 is proposed to increase by 40% to be more reflective to the actual strain hardening capacity exhibited from experiment. The revised *Point 3* is [0.035, 1.05]. The final values for parameter ε_f and σ_f/σ_{pc} of the tensile function used in the modification 2 analysis are summarised in Table 5.

Figure 8 shows the simulated tensile stress strain curves using modification 2 parameter ε_f and σ_f/σ_{pc} in the FE model. It can be observed that the simulated curve at first cracking strength and initial hardening part within 1% of strain capacity are in good agreement with the experiment responses. However, when exceeded 1% strain capacity, the prediction does not provide reasonable accuracy and deviate away from the experiment results. This implied further model calibration is still needed.

Table 5 Parameter ε_f and σ_f/σ_{pc} for modification 2

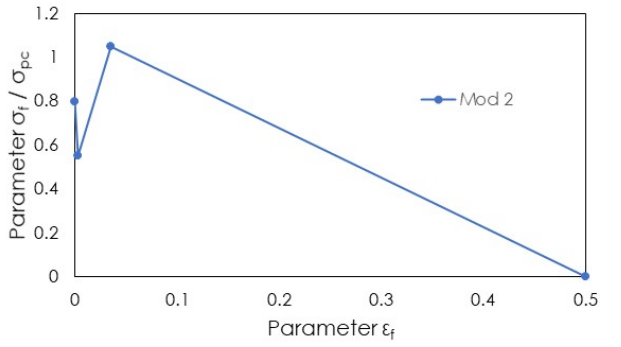

Point	Parameter ε_f	Parameter σ_f/σ_{pc}
1	0.0	0.8
2	0.0025	0.55
3	0.035	1.05
4	0.5	0

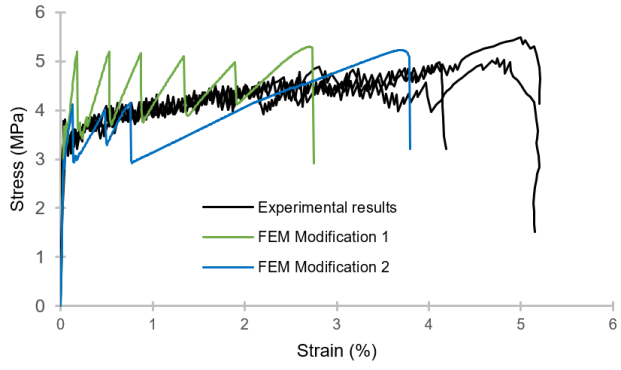

Figure 8 Comparison of tensile stress strain curves with parameter modification 1 & 2

c) Modification 3

Same procedures with preceding parameter modifications are carried out. Additional points are added on the parameter ε_f and σ_f/σ_{pc} of the tensile function in order to attain satisfactory tensile strain hardening responses. The proposed final values for parameter ε_f and σ_f/σ_{pc} are ummarized in Table 6. The results from modification 3 are illustrated in Figure 9 with comparison to the experimental results. As can be seen, the simulated model predicted fairly accurate to the experiment tensile stress, tensile strain capacity and hardening behaviour.

Figure 10 illustrate the sequence of cracking from the uniaxial tensile test simulation. It noticed that matrix cracking took place simultaneously in multiple elements within 1.0% of strain, causing a sudden drop of stress in the simulated curves shown in Figure 9. At ultimate failure, majority of the elements undergoes strain hardening with crack opening lower than δ_{pc} of 110 μm. It should be noted that final mode of failure is localized cracks happened at the lower part of the test region adjacent to the bottom support.

Table 6 Parameter ε_f and σ_f/σ_{pc} for modification 3

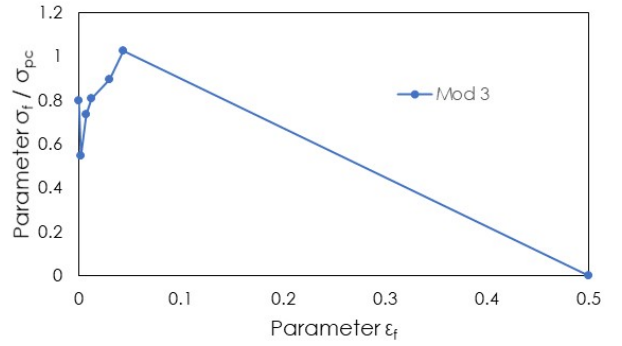

Point	Parameter ε_f	Parameter σ_f/σ_{pc}
1	0.0	0.8
2	0.0025	0.55
3	0.00712	0.7349
4	0.0124	0.8068
5	0.0296	0.8949
6	0.0437	1.0272
7	0.5	0

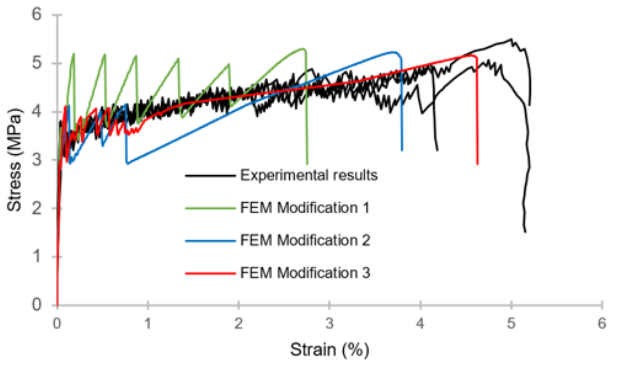

Figure 9 Comparison of tensile stress strain curves with parameter modification 1, 2 and 3

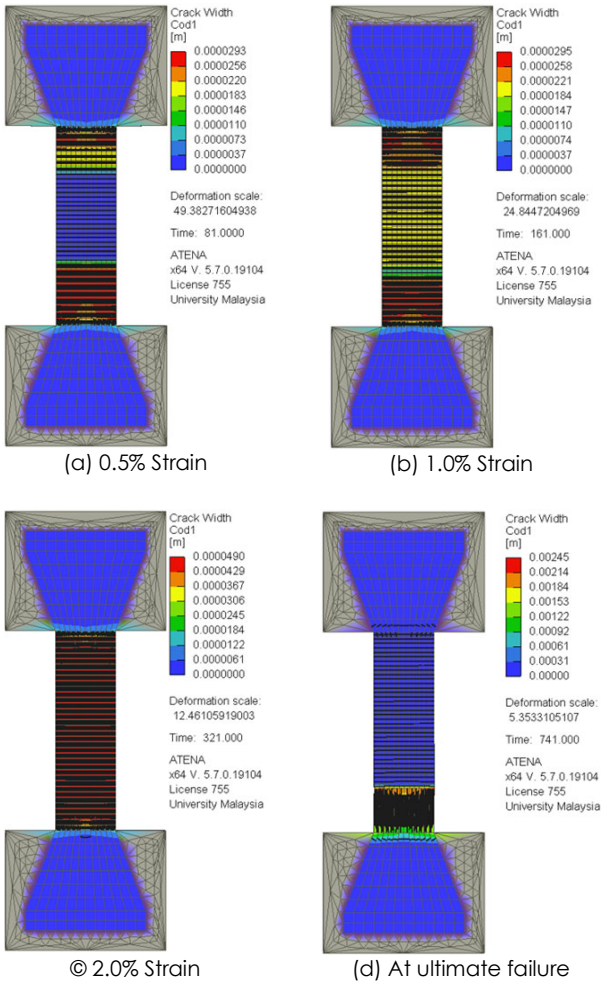

Figure 10 Development of cracking at various strain levels for uniaxial tensile test simulation using parameter modification 3

2.3.6 *Mesh Sensitivity*

It has been reported that the mesh size has great effect on the mechanical behaviour (such as load-deformation responses) of concrete material model in numerical simulation [25, 26]. Incorrect convergence in solving nonlinear equation may be obtained when an inappropriate mesh size is used in the simulation. In this study, uniaxial tensile simulations under displacement controlled were carried out using various sizes of hexahedral meshes, namely: 2.5 mm, 5 mm and 10 mm. The parameter ε_f and σ_f/σ_{pc} shown in Table 6 were used as the input parameter to generate the simulation. It is noteworthy that the characteristic length L_t used in this analysis is based on the exact studied mesh size (as mentioned in section 4.2).

The results of the studies under different mesh sizes are illustrated in Figure 11, together with the experiment curves for comparison. It is obvious that finer element led to negligible differences in the overall tensile strain hardening response. With coarser mesh, the element in the model had convergence issue in the post-peak when crack initiates.

Figure 12 shows the average crack width development between experiment and simulated results with different mesh sizes. It can be observed that coarser mesh size generated higher formation of crack widths. In contrast, finer mesh size has reduced crack widths so that constant fracture energy can be maintained. The result of the average crack width – strain curves with 2.5 mm was fairly accurate compared to the experimental results. The simulated results with the mesh sizes of 5 mm and 10 mm, on the other hand, are not in good agreement with the experimental results. Therefore, mesh size of 2.5 mm will be recommended to be used in the numerical simulation.

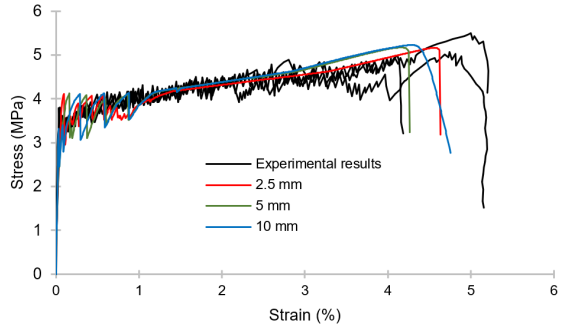

Figure 11 Stress strain curves of experimental and simulation results with different meshes

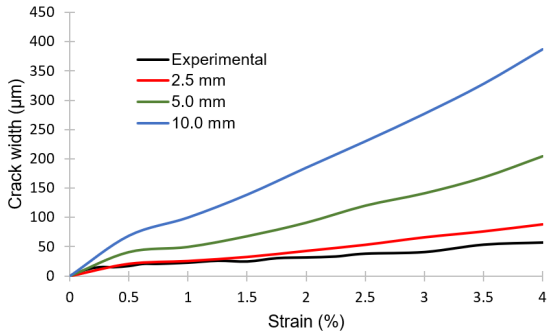

Figure 12 Average crack width development of experimental and simulation results with different meshes

3.0 RESULTS AND DISCUSSION

The performance of the adopted calibration approach described in preceding section for simulating tensile strain hardening behaviour are further validated with more experimental results. The works by Choi *et al*. [27], Magalhaes *et al*. [28], Li *et al*. [29], Ding *et al*. [30], Lu *et al*. [31] and Nematollahi *et al*. [32] are chosen for the verification. All specimens chosen to have tensile properties enhanced by PVA fibres and with dogbone-shaped size and geometry based on JSCE standard [24], see Figure 4. FE simulations are carried out using the proposed modelling technique with 2.5 mm mesh size

as described in previous section. The modelling parameters for all chosen specimens are summarised in Table 7.

Choi *et al*. [27] investigated the effect of using recycled aggregates on strain hardening cement-based materials (SHCC). Two specimens PVA2.0 and PVA2.0FA20 are chosen to carry out the simulation as both specimens indicates good performance in term of strain hardening behaviour. The numerical simulation and experimental results for tensile stress strain curves are shown in Figure 13.

Magalhaes *et al*. [28], Li *et al*. [29] and Ding *et al*. [30] studied the strain hardening behaviour of ECC. Their mix proportions are almost identical where combined mixture of cement and fly ash are used as binder. Figure 14 – 16 shows their respective tensile stress strain curves obtained from FE simulation and experimental results.

The mix proportion adopted in the specimen tested by Lu *et al*. [31] was similar to Yu *et al*. [23]. The numerical and experimental results for the tensile stress strain curves are shown in Figure 17.

Nematollahi *et al*. [32] investigated the effect of different concentration of alkaline activator on the strain hardening behaviour of fibre reinforced Engineered Geopolymer Composites (EGC) under uniaxial tension. Their simulated tensile stress strain curves along with the experimental results are plotted in Figure 18.

Generally, all tensile stress strain curves simulated from FE models agreed well with the experimental results, especially on predicting the trends and responses. It should be noted that based on observations, test results from direct uniaxial tensile tests are highly variable even from same batch of mixture and test series. Despite such variation, simulated models are still able to predict reasonably the average responses of the anticipated tensile strain hardening behaviour.

Table 7 Summary of FE model parameters

Author	Specimen	FE model parameter			
		f_c (MPa)	σ_{pc} (MPa)	E_m (GPa)	L_t (mm)
Choi *et al*. [27]	PVA2.0	23.48	2.8	10.8	2.5
	PVA2.0FA20	18.53	3.38	11.06	2.5
Magalhaes *et al*. [28]	M05	36.27	2.98	19	2.5
Li *et al*. [29]	Specimen 1-3	35	4.5	15.1	2.5
Ding *et al*. [30]	PVA-ECC	35.3	3.1	15	2.5
Lu *et al*. [31]	PVA-SHCC	35	2.12	20	2.5
Nematollahi *et al*. [32]	EGC20	63.7	4.7	8.6	2.5
	EGC23	52.6	4.3	4.8	2.5
	EGC23-FS-30	56.8	5.0	5.7	2.5

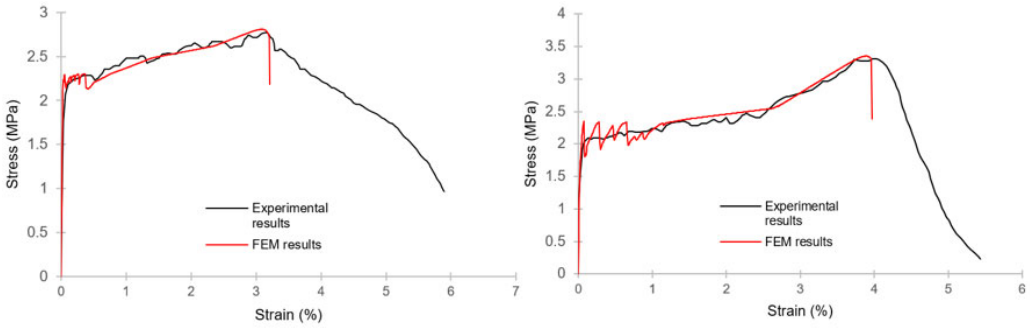

(a) PVA2.0 (b) PVA2.0FA20

Figure 13 Simulated and experiment tensile stress strain curve tested by Choi *et al*. [27].

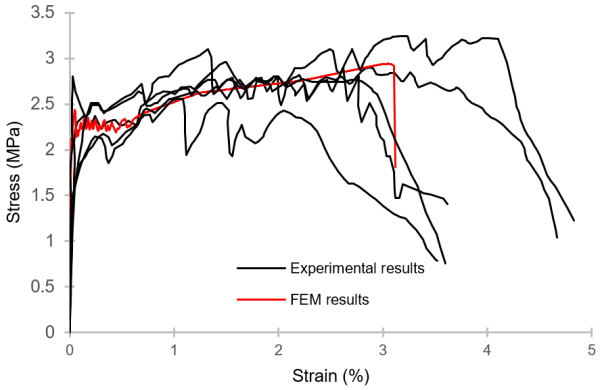

Figure 14 Simulated and experiment tensile stress strain curves tested by Magalhaes *et al*. [28]

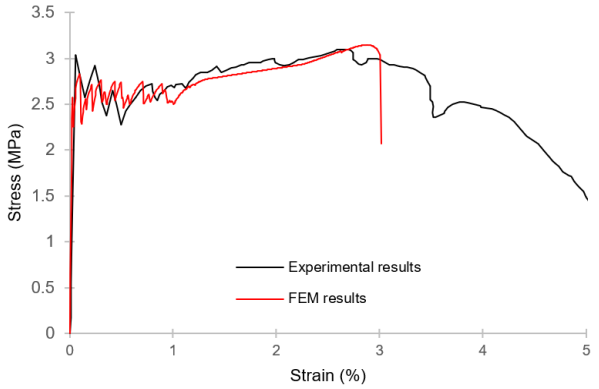

Figure 16 Simulated and experiment tensile stress strain curves tested by Ding *et al*. [30]

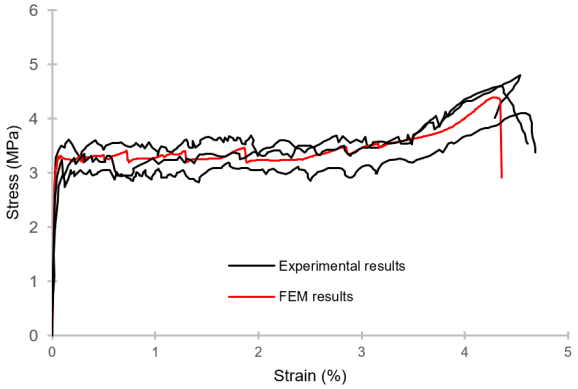

Figure 15 Simulated and experiment tensile stress strain curves tested by Li *et al*. [29]

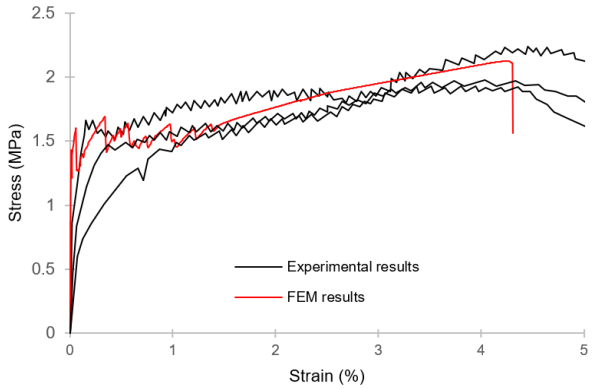

Figure 17 Simulated and experiment tensile stress strain curves tested by Lu *et al*. [31]

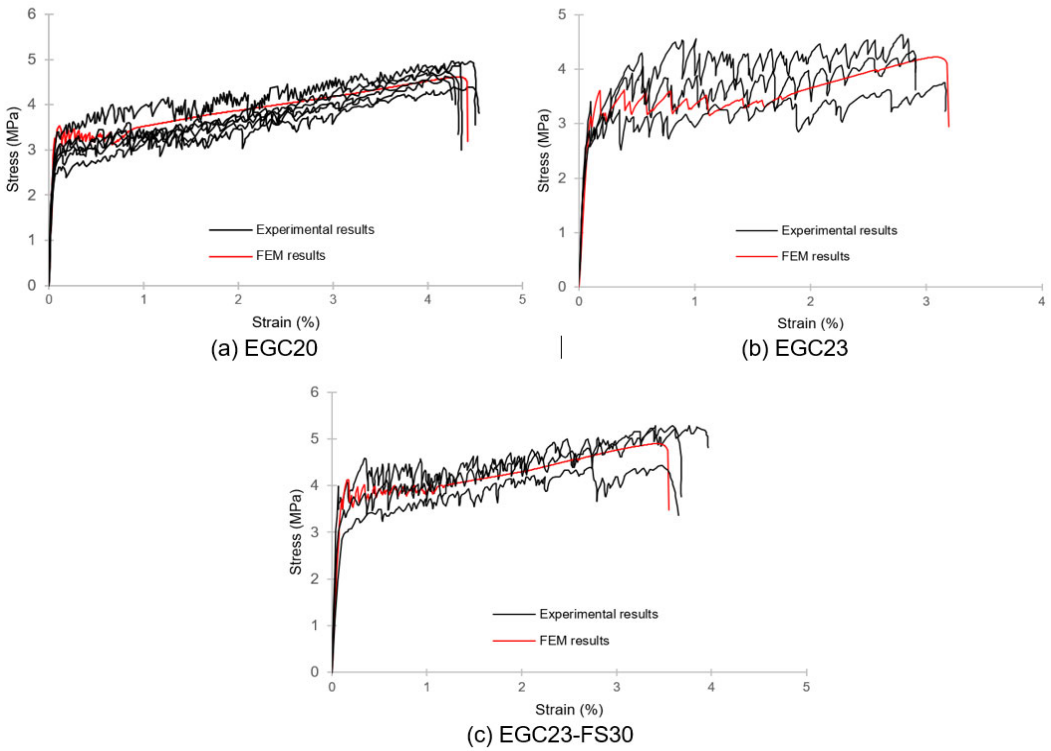

Figure 18 Simulated and experiment tensile stress strain curves tested by Nematollahi *et al*. [32]

Table 8 summarises the values of ultimate tensile strengths and strains obtained from experimental and numerical simulation. Also included in the table are the respective experimental to numerical simulation ratios for strength ($\sigma_{pc,exp}$ / $\sigma_{pc,FEM}$) and strain ($\varepsilon_{pc,exp}$ / $\varepsilon_{pc,FEM}$). Overall, $\sigma_{pc,exp}$ / $\sigma_{pc,FEM}$ and $\varepsilon_{pc,exp}$ / $\varepsilon_{pc,FEM}$ ratios are in the range from 0.98 to 1.03 and 0.90 to 1.05 respectively. It is clearly indicated that there is good agreement between experimental and numerical results with average $\sigma_{pc,exp}$ / $\sigma_{pc,FEM}$ and $\varepsilon_{pc,exp}$ / $\varepsilon_{pc,FEM}$ ratios of 1.01 and 0.99 respectively.

Figure 19 (a) and (b) plotted the numerical results versus experimental results for the ultimate tensile strength and strain capacity. Based on the observation, the results showed very good distribution along the target line, with all data points lie within ±10% bounds.

Table 8 Summary of simulation results

Specimen	$\sigma_{pc,exp}$	$\varepsilon_{pc,exp}$	$\sigma_{pc,FEM}$	$\varepsilon_{pc,FEM}$	$\sigma_{pc,exp}$/ $\sigma_{pc,FEM}$	$\varepsilon_{pc,exp}$/ $\varepsilon_{pc,FEM}$
P20 [23]	5.17	4.63	5.16	4.56	1.00	1.02
PVA2.0 [27]	2.80	3.11	2.81	3.08	1.00	1.01
PVA2.0FA20 [27]	3.38	3.70	3.35	3.89	1.01	0.95
M05 [28]	2.98	2.90	2.94	3.05	1.01	0.95
Specimen 1-3 [29]	4.50	4.50	4.39	4.29	1.03	1.05
PVA-ECC [30]	3.10	2.60	3.15	2.88	0.98	0.90
PVA-SHCC [31]	2.12	4.13	2.12	4.25	1.00	0.97
EGC20 [32]	4.70	4.30	4.60	4.33	1.02	0.99
EGC23 [32]	4.30	3.00	4.22	3.08	1.02	0.97
EGC23-FS30 [32]	5.00	3.60	4.90	3.43	1.02	1.05
				Mean =	**1.01**	**0.99**

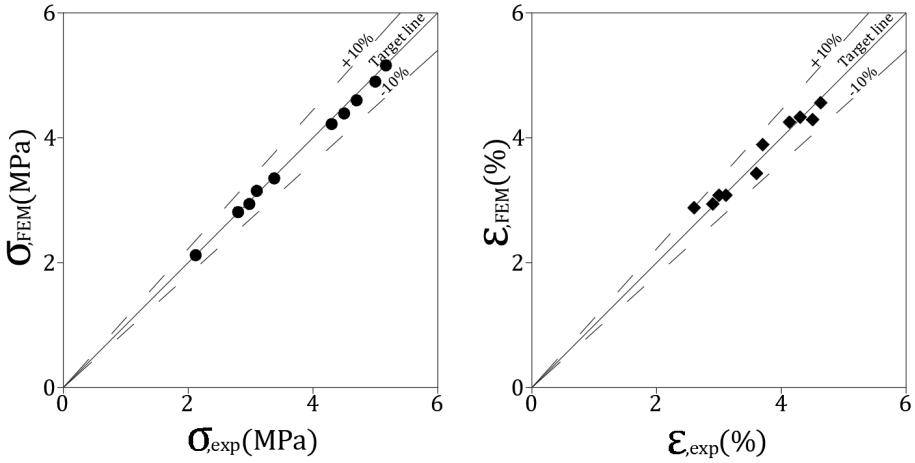

Figure 19 Simulated results obtained plotted against corresponding experimental results

4.0 CONCLUSION

In this study, the ATENA program was used to simulate the tensile strain-hardening behaviour of ECC. A finite element model to determine the multiple-cracking and tensile strain hardening behaviour of ECC was developed. "Cementitious2SHCC" was used as a material model implementation in ATENA for numerical modelling. The finite element model and calibration approach was developed based on traction separation law by calibrating the parameters such as the cracking strengths and its corresponding crack opening displacements. Simulated tensile stress-strain curves predict with reasonable accuracy the actual tensile strain hardening behaviour of ECC in terms of tensile strain capacity, first cracking strength, ultimate tensile strength, and strain hardening response using the proposed modelling and calibration technique. The accuracy of the simulated tensile strain hardening curves was found to improve by lowering the crack opening displacement corresponding to the first cracking. The proposed model has been successfully validated from 10 ECC specimens tested by various researchers. These simulated tensile stress-strain results are found to be in good agreement with the experimental results, which demonstrated the accuracy and adequacy of the proposed technique.

Acknowledgement

This research was fully supported in part by Ministry of Higher Education (MOHE) through Fundamental Research Grant Scheme

(FRGS/1/2018/TK01/HWUM/02/3) under the title of "*A Novel Cement-less Ductile Engineered Geopolymer Composites (EGC) for Sustainable Structural Applications*" and in part by the 2020 MAEDA Foundation Research Grant through with Hokkaido University, Japan.

References

[1] V. C. Li. 1998. Engineered Cementitious Composites - Tailored Composites through Micromechanical Modeling, Fiber-Reinforced Concrete: Present and the Future. N. Banthia, A. Bentur and A. Mufri. Eds. Montreal, Canada, Canadian Society of Civil Engineering. 64-97.

[2] V. C. Li, C. K. Y. Leung. 1992. Steady State and Multiple Cracking of Short Random Fiber Composites. *J. Eng. Mech. ASCE*. 188(11): 2246-2264.

[3] V. C. Li, H. Stang, H. Krenchel. 1993. Micromechanics of Crack Bridging in Fiber Reinforced Concrete. *Mater. Struct*. 26(162): 486-494.

[4] V. C. Li, T. Kanda. 1998. Engineered Cementitious Composites for Structural Applications. *J. Mater. Civ. Eng*. 10(2): 66-69.

[5] V. C. Li. 2003. On Engineered Cementitious Composites (ECCs). *J. Adv. Concr. Technol*. 1(3): 215-230.

[6] E. -H. Yang, Y. Yang, V. C. Li. 2007. Use of High Volumes of Fly Ash to Improve ECC Mechanical Properties and Material Greenness, *ACI Mater. J*. 104(6): 620-628.

[7] Z. F. Pan, C. Wu, J. Z. Liu, W. Wang, J. W. Liu. 2015. Study on Mechanical Properties of Cost-Effective Polyvinyl Alcohol Engineered Cementitious Composites (PVA-ECC). *Constr. Build. Mater*. 78: 397-404.

[8] V. C. Li, C. Wu, S. X. Wang, A. Ogawa, T. Saito. 2002. Interface Tailoring for Strain-Hardening Polyvinyl Alcohol Engineered Cementitious Composites (PVA-ECC). *ACI Mater. J*. 99(5): 463-472.

[9] V. C. Li, S. X. Wang, C. Wu. 2001. Tensile Strain-Hardening of Polyvinyl Alcohol Engineered Cementitious Composites (PVA-ECC). *ACI Mater. J*. 98(6): 483-492.

[10] K. Q. Yu, Y. C. Wang, J. T. Yu, S. L. Xu. 2017. A Strain-hardening Cementitious Composites with the Tensile Capacity Up to 8%. *Constr. Build. Mater*. 137: 410-419.

[11] *fib Model Code for Concrete Structures 2010*. Ernst & Sohn Publishing Company.

[12] T. Huang, Y. X. Zhang. 2016. Numerical Modelling of Mechanical of Engineered Cementitious Composites under Axial Tension. *Comput. Struct*. 173: 95-108.

[13] 2010. *ABAQUS Analysis User's Manual.* Providence, RI, USA: Dassault Systems Simulia Corp.

[14] P. Kabele. 2002. Continuum Model of Multiple Cracking. *Engineering Mechanics (Association for Engineering Mechanics, Czech Republic)*. 9(1/2): 75-90.

[15] P. Kabele, T. Kanakubo. 2007. Experimental and Numerical Investigation of Shear Behaviour of PVA-ECC in Structural Elements. H. W. Reinhardt & A. E. Naaman (eds.). *RILEM Proceedings of the Fifth International Workshop on High Performance Fiber Reinforced Cementitious Composites (HPFRCC5)*. Mainz, Germany, 10-13 July.

[16] P. Kabele. 2009. Finite Element Fracture Analysis of Reinforced SHCC Members. G. P. A. G. van Zijl & W. P. Boshoff (eds.). *Proc of the International Conference on Advanced Concrete Materials*. 237-244.

[17] Z. Prochazkova, J. Cervenka, Z. Janda, D. Pryl, J. Mikolaskova. 2019. ATENA Program Documentation Part 4-6: ATENA Science-GiD Tutorial. Prague: Cervenka Consulting.

[18] A. Naaman, H. Reinhardt. 2003. Setting the Stage: Toward Performance based Classification of FRC Composites. *Proceedings of 4th RILEM Symposium on High Performance Fiber Reinforced Cement, Composites (HPFRCC4)*.

[19] V. C. Li. 2012. Tailoring ECC for Special Attributes: A Review. *Int. J. Concr. Struct. Mater.* 6(3): 135-144.

[20] T. Kanda, V. C. Li. 2006. Practical Design Criteria for Saturated Pseudo Strain Hardening Behaviour of ECC. *J. Adv. Concr. Technol*. 4(1): 59-72.

[21] V. Cervenka, L. Jendele, J. Cervenka. 2020. ATENA Program Documentation Part 1: Theory, Prague: Cervenka Consulting.

[22] P. Kabele. 2007. Multiscale Framework for Modelling of Fracture in High Performance Fiber Reinforced Cementitious Composites. *Eng. Fract. Mech*. 74: 194-209.

[23] J. Yu, J. Yao, X. Y. Lin, H. D. Le, J. Y. K. Lam, C. K. Y. Leung, I. M. L. Sham, K. M. Shih. 2018. Tensile Performance of Sustainable Strain-hardening Cementitious Composites with Hybrid PVA and Recycled PET Fibers. *Cem. Concr. Res*. 107: 110-123.

[24] 2008. Concrete Engineering Series 82, Recommendations for Design and Construction of High Performance Fiber Reinforced Cement Composites with Multiple Fine Cracks (HPFRCC). Japan: Concrete Committee, Japan Society of Civil Engineers.

[25] X. S. Lin, Y. X. Zhang and P. J. Hazell. 2014. Modelling the Response of Reinforced Concrete Panels under Blast Loading. *Mater. Des.* 56: 620-628.

[26] H. Yin, K. Shirai and W. Teo. 2019. Finite Element Modelling to Predict the Flexural Behaviour of Ultra-high Performance Concrete Members. *Eng. Struct.* 183: 741-755.

[27] W. C. Choi, H. D. Yun, J. W. Kang, S. W. Kim. 2012. Development of Recycled Strain-hardening Cement-based Composite (SHCC) for Sustainable Infrastructures. *Compos. B.* 43: 627-635.

[28] M. d. S. Magalhaes, R. D. T. Filho, E. d. M. R. Fairbairn. 2014. Influence of Local Raw Materials on the Mechanical Behaviour and Fracture Process of PVA-SHCC. *Mater. Res.* 17(1): 146-56.

[29] J. Li, M. Q. Sun, J. H. Hu, R. T. Ruan, Y. J. Wang. 2016. Structural Performance of Reinforced Strain Hardening Cementitious Composites Pipes during Monotonic Loading, *Constr. Build. Mater.* 114: 794-804.

[30] Z. Ding, J. C. Wen, X. Q. Li, J. Fu, X. F. Ji. 2020. Mechanical Behaviour of Polyvinyl Alcohol-Engineered Cementitious Composites (PVA-ECC) Tunnel Linings Subjected to Vertical Load. *Tunn. Undergr. Space Technol.* 95: 10.

[31] C. Lu, J. Yu, C. K. Y. Leung. 2018. Tensile Performance and Impact Resistance of Strain Hardening Cementitious Composites (SHCC) with Recycled Fibers. *Constr. Build. Mater.* 171: 566-76.

[32] B. Nematolloahi, J. Sanjayan, F. U. A. Shaikh. 2016. Matrix Design of Strain Hardening Fibre Reinforced Engineered Geopolymer Composite. *Compos. B.* 89: 253-265.